Bulletin of the Seismological Society of America, Vol. 69, No. 6, pp. 1903–1916, December 1979

SOURCE PROCESSES OF THE HAICHENG, CHINA EARTHQUAKE FROM OBSERVATIONS OF *P* AND *S* WAVES

By John Cipar

ABSTRACT

The Haicheng, China earthquake of February 4, 1975, was the first major seismic event to be predicted. In this paper, long-period teleseismic *P* waves and *S* waves from this event are compared directly to time-domain synthetic seismograms to infer the source parameters. Results indicate the focal mechanism of the earthquake is nearly left-lateral strike slip along a northwest striking nodal plane (strike = 288°, dip = 78° N, rake = 342°). The strike of this nodal plane agrees with the trend of the aftershock distribution. Seismic moment is 3 × 10^{26} dyne-cm and source duration is 7 sec. Azimuthal variation of *P*-wave duration is attributed to fault propagation in a northwesterly direction along the strike of the aftershock zone. A model with a fault length of 22 km and rupture velocity of 3.2 km/sec can explain the observed *P* waves quite well. There is considerable discrepancy between observed *SH* waves and synthetics computed using this model. These discrepancies are due to source structure complexities and/or changes of fault mechanism as the rupture propagated along strike. The average dislocation is computed to be 2.8 m and the stress drop is 53 bars.

Introduction

The Haicheng, Liaoning Province, China earthquake of February 4, 1975, was the first major earthquake to have been successfully predicted (Raleigh *et al.*, 1977). Using a wide range of observations, principally tilt measurements and seismicity, Chinese seismologists continually improved their estimate of the time and location of the impending event.

By 1970, long-term trends in seismicity suggested to Chinese seismologists that Liaoning Province, in northeastern China, would be the site of the next large event in a series of earthquakes which began in 1966. During this series, epicenters of large earthquakes (1966 Hsingtai earthquakes, 1967 Tientsin, and 1969 Pohai Gulf) migrated northeastward toward Liaoning Province. This long-term prediction led to increased geophysical studies in Liaoning Province such as new seismic stations and tilt observations. In late 1973, the number of small earthquakes showed a significant increase in frequency while previously slow ground tilting accelerated. These geophysical observations spurred provincial authorities to make preparations for a major disaster and to step up their program of alerting citizens. Foreshock activity, beginning on February 1 and continuing up until 6 hr before the main shock, appears to have been the deciding factor in predicting the earthquake and warning the populace. From the amount of damage to homes and other buildings the prediction of this earthquake undoubtedly saved many thousands of lives. Scholz (1977) has suggested that the series of large earthquakes including the Haicheng earthquake and its precursory phenomenon were triggered by a deformation front propagating through northeastern China. The main shock occurred at 11h 36m UTC on February 4, 1975 with a surface-wave magnitude of 7.4 (USGS). Basic parameters of the main shock are listed in Table 1.

This paper is concerned with the interpretation of the source processes of the Haicheng earthquake by analysis of teleseismic body waves. In particular, the agreement between *P*-wave and *S*-wave observations will be investigated. The

method employed will be to construct synthetic seismograms in the time domain using a plane-wave approximation to generalized ray theory for shear dislocation sources (Langston and Helmberger, 1975) and to compare these synthetics directly to the observations. In this way, source parameters such as seismic moment, fault dip, rake, strike, source depth, and source time function can be estimated. Although this work does not deal specifically with earthquake prediction, the information presented should be of help in evaluating earthquake prediction data. Specifically, it may be of interest to compare this rupture model for the Haicheng earthquake to source models for other earthquakes that were not preceeded by premonitory tilt and seismicity.

Geological and Seismological Setting

Geomorphologically, Liaoning Province consists of a sediment filled central valley trending northeast-southwest flanked on either side by mountainous regions. The

TABLE 1

Main Shock Parameters

Date: February 4, 1975
Origin Time: 11h 36m 07.5s UTC (USGS)
Location: Liaoning Province, China
40.6°N, 122.6°E (USGS)
40.65°N, 122.8°E (Gu *et al.*, 1976)
Depth: Normal focal depth (USGS)
12 km (Gu *et al.*, 1976)
Magnitude:
$m_b = 6.4$, $M_S = 7.4$ (USGS)
$M = 6.7$ (PAS)
Fault Mechanism:*
strike = 288°
dip = 78°N
rake = 342°

* Coordinate system from Langston and Helmberger (1975).

central valley is bounded on the south by Pohai Gulf while the eastern mountains extend southwestward into the Gulf to form Liaotung Peninsula (Figure 1). Numerous northeast striking faults showing evidence of recent movement have been mapped on Liaotung Peninsula and in the mountains to the north (Raleigh *et al.*, 1977). These faults are believed to be extensions of a system of strike-slip faults in Shantung Province south of Pohai Gulf. The 1969 Pohai Gulf earthquake ($M_S = 7.4$) is evidence that this fault system is presently active.

The Haicheng earthquake occurred near the contact between the central valley and the eastern mountains. However, the aftershock distribution map (Figure 2) derived from local data (Gu *et al.*, 1976), indicates that the faulting did not take place on one of the northeast trending faults but occurred on a fault plane aligned west-northwest. According to Hsu (1976), the aftershocks covered an area about 70 by 30 km and most were shallower than 12 km. A cross section of aftershock hypocenters normal to the strike of the distribution shows that the aftershocks define an almost vertical plane (Figure 3 of Hsu, 1976). The aftershock distribution is aligned very well with the west-northwest striking nodal plane of the teleseismic *P*-wave first-motion diagram (Figure 3). This diagram, which was constructed using long-period WWSSN data, agrees closely with the mechanism derived from local data (Hsu, 1976). The first-motion diagram indicates predominantly strike-slip

motion on nearly vertical fault planes. Choosing the west-northwest striking plane as the fault plane, the motion is left lateral with the following parameters: strike = 288°, dip = 78°N, rake = 342° (sign convention for the fault mechanism is that of Langston and Helmberger, 1975). Mechanisms of the aftershocks (Gu *et al.*, 1976) are very similar to the main shock mechanism. The main shock focal depth estimate of 10 km from teleseismic data agrees well with the 12-km depth computed from local observations.

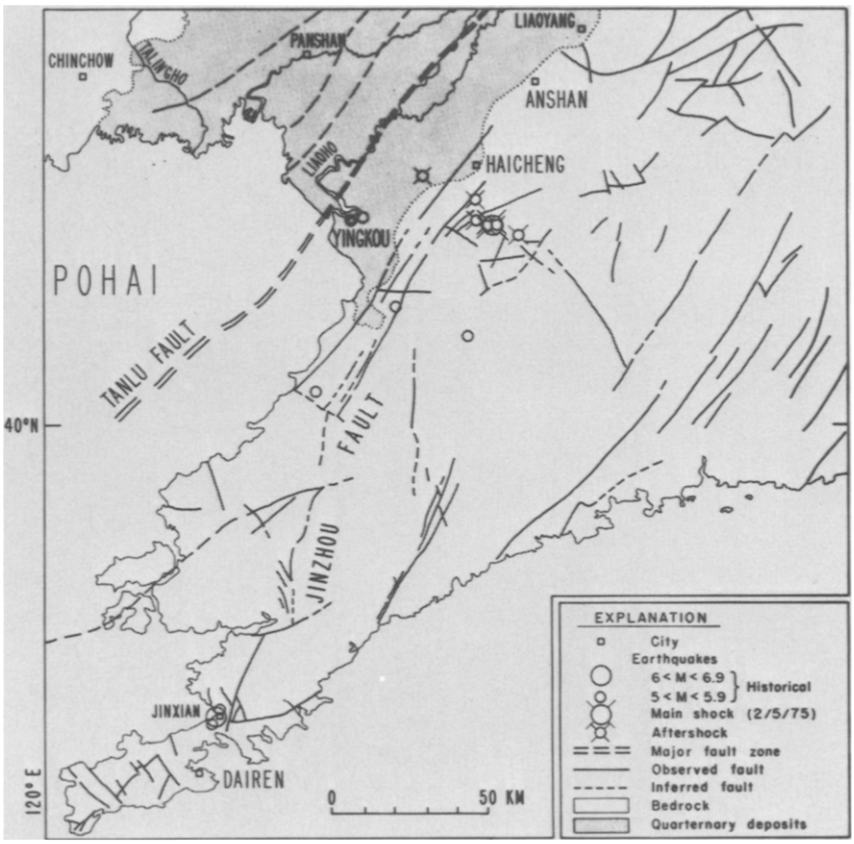

FIG. 1. Generalized geological map of Liaoning Province showing mapped faults and epicenters of the Haicheng earthquake and its aftershocks. Stippled area is a Quaternary sedimentary basin; dotted lines are edges of the basin (after Raleigh *et al.*, 1977).

DATA

The Haicheng earthquake was well recorded by WWSSN stations around the world and a good collection of on-scale records is available. *P*-wave polarities were read from long-period WWSSN vertical seismograms and plotted on the focal mechanism (Figure 3) discussed above. Twelve *P*-wave and nine *S*-wave records were selected for further study based on clarity of recording and absence of long-period noise. To minimize complications due to upper mantle structure and core effects, only stations within the distance range 30° to 85° were used. Also, stations with obvious *PL* waves were eliminated.

The seismograms were digitized on an electronic digitizing table and then detrended, deskewed, interpolated, and plotted at a uniform magnification and time

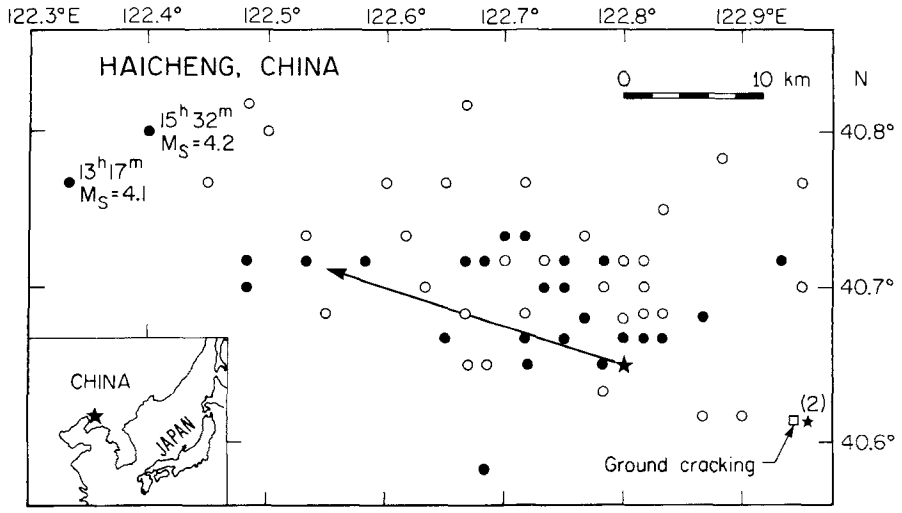

FIG. 2. Map of aftershock distribution. Star marks the main shock epicenter. Closed circles are aftershocks which occurred within 1 day of the main shock; open circles are later aftershocks. The main shock occurred at 11h 36m UTC. Times of the two aftershocks which occurred within 4 hr of the main shock at the northwest end of the aftershock zone are indicated. Data is from Gu *et al.* (1976). Heavy line indicates length and direction of fault propagation inferred from *P* waves. Locality of ground cracking is reported by Raleigh *et al.* (1977).

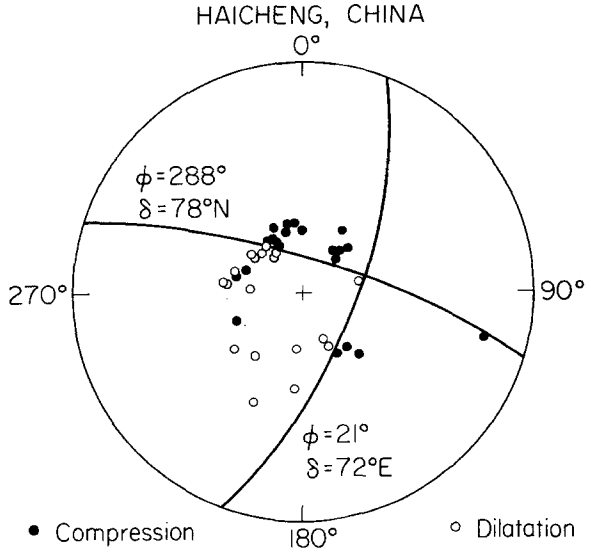

FIG. 3. Teleseismic *P*-wave first-motion diagram plotted on lower half of focal sphere. Observations read on WWSSN long-period vertical seismographs.

scale by computer. In the case of *S* waves, both N-S and E-W components were digitized and numerically rotated to produce *SH* and *SV* waves. Station information and *P*-wave first motions are listed in Table 2.

THEORY

Application of generalized ray theory for shear dislocations to the study of teleseismic body waves of earthquakes is set forth in Helmberger (1974) and Langston and Helmberger (1975). Briefly, a far-field synthetic seismogram for a point source in a layered medium can be constructed by adding up the contribution

TABLE 2

STATION DATA

Station	Distance (deg)	Azimuth (deg)	Back Azimuth (Deg)	*P*-Wave Reading*	Synthetic
AAE	79.7	273.2	50.2	i–	*P, S*
ADE	76.7	166.6	347.6	e+	*S*
ATU	72.4	305.2	51.9	i–	*P, S*
AFI	81.2	116.5	315.5	node	*S*
COR	76.5	42.1	314.4	e+	*S*
GDH	70.4	358.6	3.0	i+	*P*
GUA	33.2	138.0	328.5	e+	*P, S*
IST	67.3	305.2	55.3	i–	*P*
MSH	48.7	286.5	64.6	i–	*P, S*
MUN	72.5	185.9	5.3	i–	*P, S*
PMG	54.7	150.0	337.4	e+	*P*
PTO	87.4	325.6	34.7	e–	*P*
RIV	78.6	156.2	338.3	e–	*P*
VAL	79.2	332.6	34.4	i+	*P, S*

* e, Emergent arrival; i, impulsive arrival; +, up first motion on vertical seismogram; –, down first motion.

of each ray in the medium and then convolving the summation with operators describing source-time history, geometrical spreading, earth attenuation, and instrument response. For instance, the teleseismic *P*-wave group for the simplest case, that of a point source at some depth within a half-space, is made up of three rays: *P*, *pP*, and *sP*. Equation (1) from Langston and Helmberger (1975) illustrates the factors involved in computing the far-field vertical response, *W*, in a half-space

$$W = \left[\dot{\phi} + Rpp\, \dot{\phi}\,(t - \Delta t_1) + \left(Rsp \frac{\eta_\alpha}{\eta_\beta} \right) \dot{\Omega}\,(t - \Delta t_2) \right] * S(t) * I(t) * Q(t) \qquad (1)$$

where

$*$ indicates the convolution operation

$\dot{\phi}$ = time derivative of the *P*-wave potential

$\dot{\Omega}$ = time derivative of the *SV* potential

Rpp = reflection coefficient at the free surface for *pP*

Rsp = reflection coefficient for *sP*

Δt_1 = time lag of *pP* relative to direct *P*

Δt_2 = time lag of *sP* relative to direct *P*

$S(t)$ = far-field dislocation time function

$I(t)$ = impulse response of the instrument

$Q(t)$ = time domain Q operator

$\eta_c = (1/c^2 - p^2)^{1/2}$, p = ray parameter,

c = seismic velocity.

Similar equations are used to construct synthetics for *SH* and *SV* waves. The radiation pattern is contained in the potentials ϕ and ψ and the depth effect comes from the time lag of *pP* and *sP* relative to direct *P*. The far-field source time function, $S(t)$, arises from the interaction of the displacement time history of two initially adjacent points located on either side of the fault plane and the finite rupture time of the earthquake. The time function appropriate for a long, slender strike-slip fault can be approximated by a trapezoid (Savage, 1972).

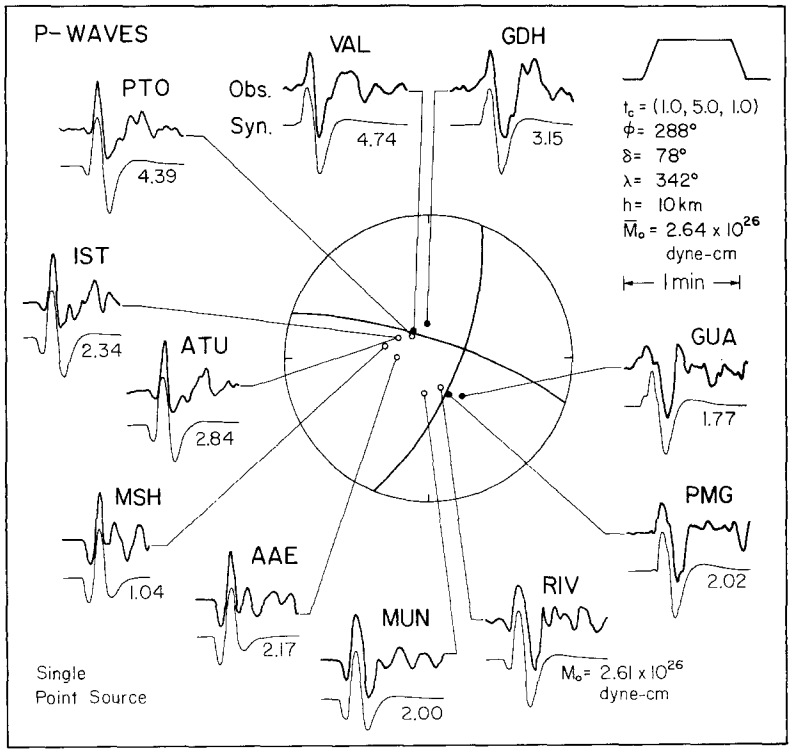

FIG. 4. Comparison of observed and synthetic *P* waves. Synthetics are computed for a point source at 10 km depth in a half-space. Far-field time function, t_c, is a trapezoid of 7-sec duration. Fault strike (ϕ), dip (δ), rake (λ), source depth (h), and average moment (M_o) are indicated.

BODY-WAVE MODELING

Preliminary synthetics for the Haicheng earthquake were constructed using a single point source in a half-space. The first step was to test the determination of source depth (h = 10 km) and focal mechanism (strike = 288°, dip = 78°N, rake = 342°) by computing synthetics for different values of each parameter and observing changes in wave shape. Source depth controls the separation of each phase (*P*, *pP*, *sP*) while the focal mechanism determines the polarity and relative amplitude of the phases. The above values for depth and focal mechanism produced the best fitting synthetics.

The major factor controlling the shape of the synthetic is the source-time function, especially the total duration. By trial and error, it was found that a trapezoidal time function of 7-sec duration with 1- to 2-sec ramps at either end produced the best overall fit to the *P*- and *S*-waveform data. The synthetic seismograms were not very sensitive to the length of the ramp part of the time function. Anelastic

attenuation effects were included in the synthetic seismogram calculations by means of Futterman's Q operator (Futterman, 1962) with $T/Q = 1.0$ for P waves and 4.0 for S waves.

Data on crustal structure in northeastern China is presently not available; however, synthetics calculated for a strike-slip source in reasonable continental structures indicate that the principle effect of structure is to modify the latter part of the waveform while not appreciably affecting the first 10 sec. For this reason, the earthquake can be modeled as a point source in a half-space. The wide variety of

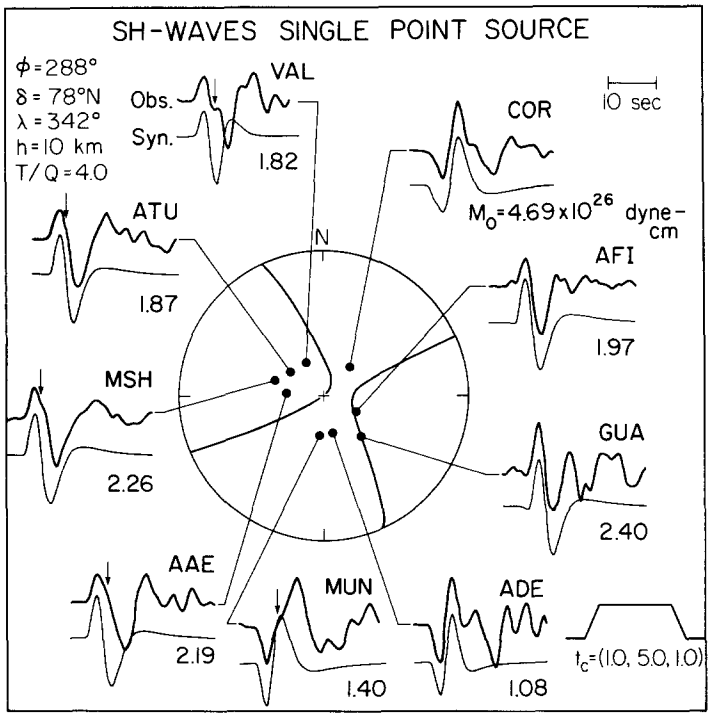

FIG. 5. Comparison of observed and synthetic *SH* waves. Synthetics are computed for a point source at 10 km depth in a half-space. Ratio of T/Q for this case is 4.0 sec. Far-field time function is a trapezoid of 7-sec duration. Arrows indicate second arrival at several stations.

receiver crusts, ranging from oceanic island to continental rift zone, precluded any attempt to model the effect of receiver crust on the synthethics.

A comparison of observed P and S waves to synthetics computed for a point source in a half-space is shown in Figures 4 and 5. The overall agreement in polarity, shape, and relative amplitude between observed data and synthetics is good indicating that the basic parameters of the model (fault mechanism, depth, time function) are reasonable and that a point source is a good approximation for this earthquake at teleseismic distances. The seismic moment is found by matching the absolute amplitudes of the observed records to the amplitudes of the synthetics.

There are features of the waveforms, however, which suggest more complex source processes. Note that observed P waves recorded at stations with easterly azimuths (GUA, PMG, RIV, MUN) tend to be longer in duration than the corresponding synthetics (Figure 4), while at stations to the west (AAE, MSH, IST, ATU), the synthetics are longer than the observed data. This can best be seen by comparing the width of the large upswing pulse at RIV and ATU, as examples. This

pulse is primarily the *sP* ray. At RIV, the observed pulse width is much broader than the synthetic while the opposite is true at ATU. To anticipate later results, this azimuthal pattern of *P*-wave duration can be explained by fault propagation from the epicenter to the northwest.

The *SH* waves (Figure 5) also show an azimuthal variation. There is good agreement between observed and synthetic waveforms at eastern stations (ADE, GUA, AFI, COR). At western stations, however, the observed *SH* waveforms are somewhat long compared to the synthetics. The anomalously long duration of the observed *SH* waves at western stations (VAL, ATU, MSH, AAE, MUN) seems to be due to a second arrival which comes in on the first downswing, about 10 sec into the record (indicated by arrows on Figure 5). The arrival is especially prominent at station VAL, while at MUN, the arrival causes severe distortion of the waveform. At stations AAE, MSH, and ATU, the arrival is seen as a "shoulder" on the first downswing and greatly lengthens the pulse. No such arrival can be seen at the eastern *SH* stations (COR, AFI, GUA, ADE) nor is the arrival apparent in the *P* waves.

A possible explanation for this second arrival is that there was a second source of radiation occurring to the southeast of the original epicenter at a slightly later time. The position to the east or southeast would explain why the phase is visible at western stations but not at eastern stations where it is hidden in the *SH* pulse from the main source.

Cipar and Hanks (1977) describe a model for the Haicheng earthquake which has a second, smaller source of radiation 13.5 km southeast of the epicenter, delayed by 4.5 sec relative to the main source. While this model improves the fits to the *SH* waves at ATU and MSH, it does not reproduce the SH waveforms observed at VAL or MUN nor are any *P*-wave fits improved. The location of the main shock epicenter near the southeast end of the aftershock zone (Figure 2) indicates that the main part of rupture propagation was to the northwest. While it is likely that there was faulting southeast of the epicenter (as indicated by surficial effects, Raleigh *et al.*, 1977), this part of the fault was probably not a major contributor to the teleseismic radiation. Also, the fact that the second source is not observable in the *P* waves at western stations, suggests that some other factor is affecting the *SH* waves at western stations.

An alternative explanation for the second arrival at western *SH* stations is near source structural complications. Nonhorizontal structures in the sedimentary basin to the west of the epicenter (Figure 1) could cause contamination of the *SH* records by *P-SV* contributions converted at the interface between the sediments and bedrock (Langston, 1977; Hong and Helmberger, 1978). To the east, there is no sedimentary basin and hence the *SH* records are not contaminated. Such structures would not severely affect the first 10 to 20 sec of the *P* wave, the portion being modeled.

It was noted above that *P*-wave duration seems to vary with azimuth in a regular way. Either a nonsymmetrical source time function or azimuthal variation of anelastic attenuation might account for the observations. Trial models using different values T/Q showed that the variation of *P*-wave duration could not be explained with any reasonable T/Q ratios. In addition, the variation seems to be quite regular: short durations recorded to the west, long durations to the east. Perhaps the simplest way to account for these observations is by means of a propagating fault which would lead to the observed azimuthal variation in the apparent teleseismic *P*-wave time function.

To model a propagating source, a set of synthetics were computed for time functions with durations from 4.0 to 11.0 sec keeping the source depth and fault mechanism fixed. At each station a synthetic was chosen which best fit the observed record. Note that for the point source model (Figure 4), one time function was used for all the records. For the propagating source case, the time function was variable from station to station. Examples of the fitting process at several stations are shown in Figure 6.

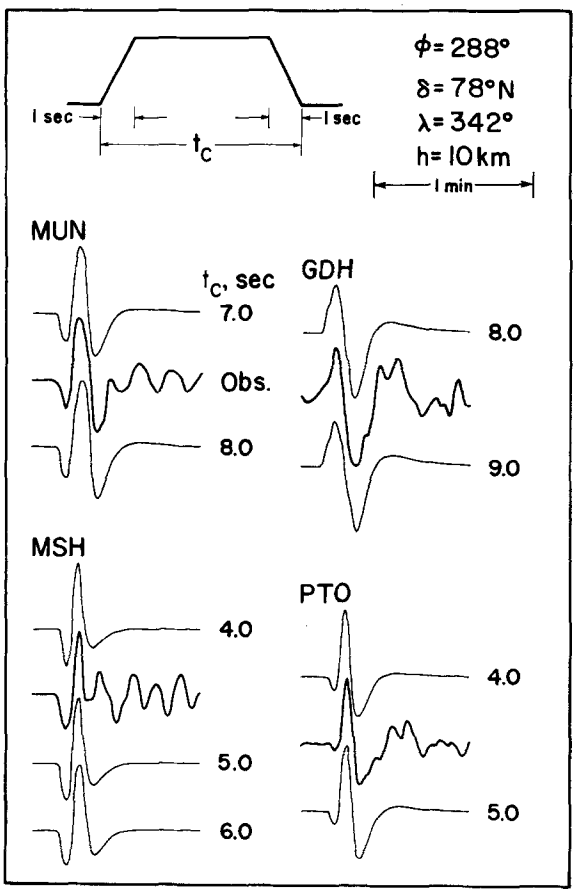

FIG. 6. Comparison of observed P waves to synthetics computed using time functions of different durations. The best fitting time functions are quite different from station to station.

The observed P waves along with the best fitting synthetics are shown in Figure 7. Note that the duration of the synthetic time function (the upper number after each synthetic) varies with azimuth and is shorter for P waves at western stations (VAL, PTO, ATU, IST, MSH) than at eastern stations (GDH, GUA, PMG, RIV, MUN). In general, the fit of the synthetics to the observed records is excellent. Even relatively minor details of the records are reproduced by the synthetics. The average seismic moment for this model is 3.15×10^{26} dyne-cm (Figure 7).

The variation of apparent P-wave function with azimuth can be easily interpreted as the effect of a propagating source. The apparent duration of the faulting process at any azimuth from a unilaterally propagating fault can be expressed as

$$t_c = (L/v_R) - (L/c) \cos \theta \tag{2}$$

where v_R = fault rupture velocity, L = fault length, c = wave velocity in source region, and θ = angle between rupture direction and ray. Using this relationship, we can interpret the observed variation of the time function with azimuth as an effect of a horizontally propagating fault as shown in Figure 8. Here the data are the observed P-wave time functions (solid circles) for each station plotted versus azimuth. The solid line connects theoretical values (open circles) computed with equation (2) for v_R = 3.2 km/sec, L = 22 km, c = 6.0 km/sec, and fault azimuth of 288°. Since the fault is assumed to propagate horizontally and the variation of ray

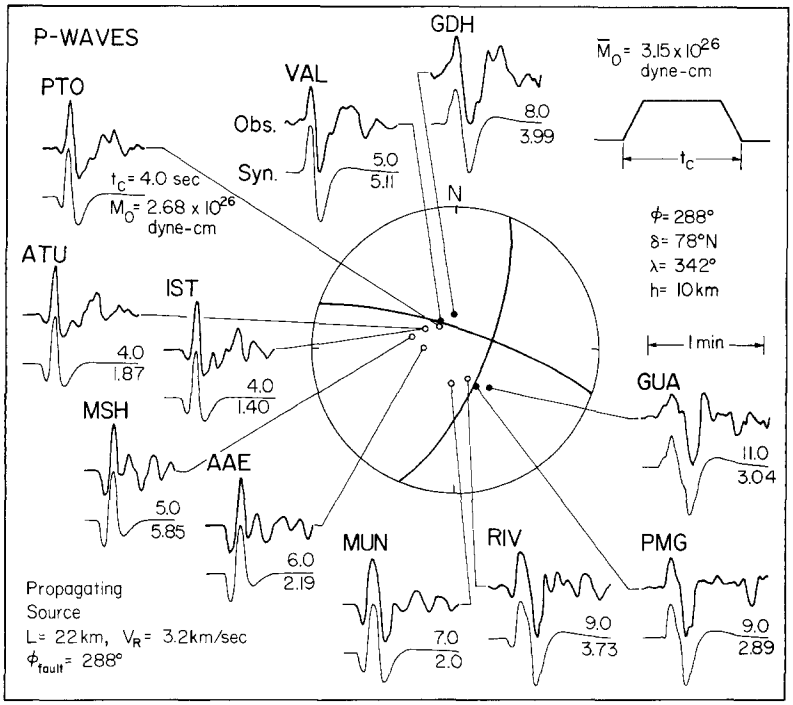

FIG. 7. Comparison of observed P waves to synthetics. In this case the duration, t_c, of the far-field time function (upper number after each synthetic) is different for each station.

takeoff angle with distance is small (less than 15°) at the ranges used, we can plot the points as a function of azimuth. The agreement between the computed and observed values for P waves is quite good.

The same procedure was applied to the SH waves with poor results as might be expected from simply looking at the observed records. In Figure 8, the closed triangles are the observed SH-wave time functions and the dashed line connects theoretical values (open triangles) calculated with the model used above. The observed SH-pattern is exactly opposite the predicted pattern.

DISCUSSION

In the previous section, it was shown that the P waves radiated by the Haicheng earthquake could be explained quite well by a propagating point source. Despite the gross simplification of aproximating the Earth by a half-space, synthetic seismograms matched the observed P waves in considerable detail. Agreement between

synthetic and real *SH* waves was much poorer. Cipar and Hanks (1977) previously attributed some of the complexities of the western *SH* waves (VAL, ATU, MSH, AAE, MUN) to a secondary source of radiation located to the southeast of the main epicenter. Another plausible explanation is complex interference and mode conversion effects in the deep sedimentary basin west of the epicenter. Based on the

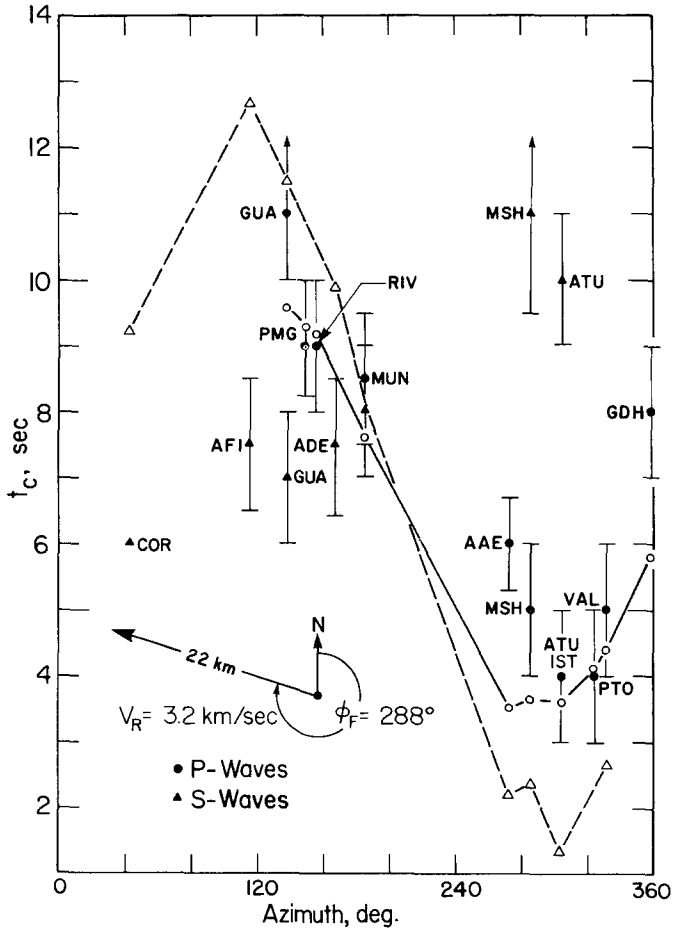

FIG. 8. Observed time function duration plotted versus azimuth for *P* wave (closed circles) and *SH* waves (filled triangles). Open circles and triangles are theoretical time-function durations for a fault propagating 22 km to the northwest at 3.2 km/sec. Solid and dashed lines show the overall form of the theoretical pattern. Error bars are estimated in the manner illustrated in Figure 6.

limited data at hand, it is not possible to conclusively assess the relative importance of either structure or source complexities on the observed waveforms.

Perhaps more disturbing is the relatively short durations of *SH* waves recorded at eastern stations (COR, AFI, GUA, ADE). At these azimuths, the propagating fault model predicts *SH* waves of long duration. Intuition might say that earth structure would lengthen waveforms and make them more complex but it is hard to imagine a structural configuration which would decrease the duration of a pulse. One might appeal to a drastic change in fault mechanism as propagation proceeded. For instance, the mechanism could change from predominantly strike-slip in the southeast to more dip-slip in the northwest. This would preserve the observed *P*-wave

first motions, but would reduce S-wave radiation relative to P for the latter part of fault propagation. We would expect to see this effect reflected in the observed surface-wave mechanism since the period of surface waves is considerably longer than the time of the whole faulting process. However, the surface-wave mechanism reported by Stewart *et al.* (1976) is consistent with the mechanism determined from body waves (Figure 3) indicating that there was no appreciable change in fault orientation. Also, aftershock focal mechanisms over the length of the zone (Gu *et al.*, 1976) are for the most part consistent with the mechanism determined for the main shock (Figure 3). Gu *et al.* (1976) do report several aftershocks with nodal planes similar to those of the main shock but with reversed polarity. In contrast to the main shock and most of the aftershocks which are left-lateral, these right-lateral events are interpreted by Gu *et al.* (1976) as the response of the fault zone to overshoot during the main shock. Because of the S-wave records, we cannot unequivocally state that we have observed fault propagation for the Haicheng earthquake. The P-wave data, however, strongly suggest that this effect is present in the records. The value of the propagating source model is that while it is a simple extension of the point source case, it leads to visible improvement in the synthetic P waves.

The 40-km length of the aftershock zone northwest of the epicenter (Figure 2) is somewhat longer than the 22-km long fault predicted by the propagating source model. An $M_S = 4.1$ aftershock (time marked on Figure 2) occurred near the northwest end of the aftershock zone within 2 hr of the main shock. This suggests that the extra 15 km of aftershocks were triggered soon after the main event and are not the normal slow diffusion of aftershocks with time (Mogi, 1968). Perhaps some kind of aseismic creep event propagated along the fault. Slow deformation during the main earthquake would probably not radiate significant energy in the body-wave frequency band but might affect long-period surface waves (e.g., Kanamori and Stewart, 1976). However, the seismic moment computed by Stewart *et al.* (1976) from surface waves is 3×10^{26} dyne-cm, the same as the moment computed from body-wave amplitudes. Perhaps the extra 10 to 15 km of aftershocks were triggered by an aseismic rupture event after the main episode of brittle faulting recorded by the body and surface waves. Burdick and Mellman (1976) report similar observations for the Borrego Mountain, California earthquake. They show that the aftershock zone is considerably larger than the region of the fault which radiated the body waves.

The average dislocation, D_0, of the Haicheng earthquake can be estimated from the formula for seismic moment, M_0 (Kanamori and Anderson, 1975): $M_0 = \mu L w D_0$ where L is the fault length, w is the fault width, and μ is the rigidity ($= 3.6 \times 10^{11}$ dynes/cm^2). The average value for M_0 is 3×10^{26} dyne-cm (Figure 7), L is about 25 km, and w is estimated to be 12 km from the depths of aftershocks. Using these values, D_0 is about 2.8 m. The stress-drop of a strike-slip fault is given by the formula (Kanamori and Anderson, 1975): $\Delta\sigma = (2/\pi)\mu(D_0/w)$ and is found to be 53 bars. Gu *et al.* (1976) estimate M_0 and $\Delta\sigma$ from field observations. Maximum horizontal offset of 55 cm was measured at Shiaokushan District (Hsu, 1976). The aftershock distribution, which presumably outlines the maximum size of the fault plane, was taken to be 70 by 20 km. Using these values, Gu *et al.* (1976) determined the moment to be 2.1×10^{26} dyne-cm and the stress drop as 4.8 bars. The discrepancy between the value of D_0 from this paper and Gu *et al.* (1976) may be due to the dying out of the dislocation as it reaches the surface. Ground cracking and related phenomena were reported in only one locality (Figure 2). The low stress drop value

computed by Gu *et al.* (1976) is a consequence of the low value of D_0 they use. The value of stress drop (53 bars) computed in this paper is well within the range of stress drops compiled by Kanamori and Anderson (1975, their Figure 1) and is typical of intraplate earthquakes.

Regarding the prediction of the Haicheng earthquake, it seems that none of the parameters estimated in this paper indicate abnormal source behavior. In particular, the stress drop is in the range reported for other shallow earthquakes and the seismic moment computed from body waves is in excellent agreement with the surface-wave moment. It is worth restating, however, several unusual features of this earthquake. First, the fault which broke during the earthquake was transverse to the regional tectonic and structural trends. Second, there was considerable aftershock activity within hours of the main shock apparently not associated with the main episode of faulting. Third, it is somewhat surprising that there was only minor surface faulting considering the large size and shallow depth of the earthquake. At present, it simply is not clear whether these phenomenon are related to the tilting and seismicity observed before the Haicheng earthquake.

Conclusions

In this paper, an interpretation of the source processes of the February 4, 1975 Haicheng, China Earthquake has been presented, based on the study of long-period teleseismic body waves. First-motion data along with synthetic seismogram calculations for *P* and *SH* waves indicate that fault motion was predominantly left-lateral strike-slip on a northwest trending plane or right-lateral on a northeast striking plane. The west northwest striking nodal plane is aligned with the strike of the aftershock distribution, implying that it is the fault plane. This fault plane is transverse to the regional topography and fault trends. Synthetic seismograms indicate the source is at a depth of 10 km. Fault width is estimated to be 12 km based on aftershock depths.

Variation of the *P*-wave far-field time function with azimuth also suggests the west-northwest focal plane is the fault plane. This variation can be interpreted by means of a fault propagating to the west northwest (azimuth = 288°) for a distance of about 22 km with a rupture velocity of 3.2 km/sec. Unfortunately, *SH*-wave records do not confirm this simple analysis. However, these *SH* waves may be contaminated by complexities in the source crustal structure. Alternatively, source complications could affect the waveforms.

The seismic moment from body waves is 3×10^{26} dyne-cm, the same as obtained from surface waves (Stewart *et al.*, 1976). Thus we can conclude that both surface waves and body waves were radiated by the same source process. The estimate of fault length of about 22 km from body waves leaves 10 to 15 km of the aftershock zone unexplained in terms of the main rupture propagation. An $M_S = 4.1$ earthquake at the northwest end of the aftershock zone (40 km from the main shock) occurred within 2 hr of the main shock. Perhaps some kind of fast creep mechanism is required to explain this observation.

Using the above values for seismic moment and fault length and width, the average dislocation is estimated to be 2.8 m. The stress drop is calculated as 53 bars, in good agreement with other intraplate earthquakes.

Acknowledgments

I wish to thank Tom Hanks who originally suggested the research and who assisted in the early phase of the investigation. Wai Ying Chung, John Ebel, Don Helmberger, and Jim Pechmann critically read

the manuscript and provided many valuable comments. Chuck Langston generously provided his computer programs for calculating synthetic seismograms. This research was supported by National Science Foundation Grant EAR78-14786.

References

Burdick, L. J. and G. R. Mellman (1976). Inversion of the body waves from the Borrego Mountain earthquake to the source mechanism, *Bull. Seism. Soc. Am.* **66,** 1485–1499.

Cipar, J. and T. C. Hanks (1977). Source parameters of the Haicheng Earthquake (abstract), *EOS, Trans. Am. Geophys. Union* **58,** 446.

Futterman, W. I. (1962). Dispersive body waves, *J. Geophys. Res.* **67,** 5279–5291.

Gu, H., Y. T. Chen, X. Gao, and Y. Zhao (1976). Focal mechanism of Haicheng, Liaoning Province, earthquake of February 4, 1975, *Acta Geophys. Sin.* **19,** 270 (in Chinese).

Helmberger, D. V. (1974). Generalized ray theory for shear dislocations, *Bull. Seism. Soc. Am.* **64,** 45–64.

Hong, T. L. and D. V. Helmberger (1978). Glorified optics and wave propagation in nonplanar structure, *Bull. Seism. Soc. Am.* **68,** 1313–1330.

Hsu, S. H. (1976). Characteristics of the Haicheng Earthquake of 1975 in *Proceedings of the Lectures by the Seismological Delegation of the People's Republic of China*, Paul M. Muller, Editor, Jet Propul. Lab., Calif. Inst. of Technol., Pasadena.

Kanamori, H. and D. L. Anderson (1975). Theoretical basis of some empirical relations in seismology, *Bull. Seism. Soc. Am.* **65,** 1073–1095.

Kanamori, H. and G. Stewart (1976). Mode of strain release along the Gibbs Fracture Zone, Mid-Atlantic Ridge, *Phys. Earth Planet. Interiors* **11,** 312–332.

Langston, C. A. (1977). The effect of planar dipping structure on source and receiver responses for constant ray parameter, *Bull. Seism. Soc. Am.* **67,** 1029–1050.

Langston, C. A. and D. V. Helmberger (1975). A procedure for modelling shallow dislocation sources, *Geophys. J.* **42,** 117–130.

Mogi, K. (1968). Development of aftershock areas of great earthquakes, *Bull. Earthquake Res. Inst., Tokyo Univ.* **46,** 175–203.

Raleigh, B., G. Bennett, H. Craig, T. Hanks, P. Molnar, A. Nur, J. Savage, C. Scholz, R. Turner, and F. Wu (1977). Prediction of the Haicheng Earthquake, *EOS, Trans. Am. Geophys. Union* **58,** 236–272.

Savage, J. C. (1972). Relation of corner frequency to fault dimensions, *J. Geophys. Res.* **77,** 3788–3795.

Scholz, C. H. (1977). A physical interpretation of the Haicheng Earthquake prediction, *Nature* **267,** 121–124.

Stewart, G. S., R. Butler, and H. Kanamori (1976). Surface and body wave analyses for the February 4, 1975 Haicheng and July 27, 1976 Tangshan Chinese Earthquakes (abstract), *EOS, Trans. Am. Geophys. Union* **57,** 953.

Seismological Laboratory
Division of Geological and Planetary Sciences
California Institute of Technology
Pasadena, California 91125
Contribution No. 3231

Manuscript received March 27, 1979